03,05

Magnetoimpedance in manganese sulfide substituted with lutetium

© M.N. Sitnikov[1], S.S. Aplesnin[1,2], A.M. Kharkov[1,¶], H. Abdelbaki[1], F.V. Zelenov[1]

[1] Siberian State University of Science and Technology,
Krasnoyarsk, Russia
[2] Kirensky Institute of Physics, Federal Research Center KSC SB, Russian Academy of Sciences,
Krasnoyarsk, Russia

¶ E-mail: khark.anton@mail.ru

Received November 11, 2022
Revised November 11, 2022
Accepted November 14, 2022

The components of the impedance, the impedance of the $Lu_xMn_{1-x}S$ ($x < 0.2$) solid solution in the temperature range of 80−500 K and the frequency of $100-10^6$ Hz were studied. A change in the sign of the magnetoimpedance in concentration and temperature is found. The contribution of the reactive and active components to the magnetoimpedance is determined. The correlation of magnetoimpedance temperatures with the temperatures of the maximum attenuation of ultrasound and electrosound has been established. The frequency dependences of the reactive part of the impedance are described in the Cole−Cole model.

Keywords: Semiconductors, impedance, magnetoimpedance, attenuation of ultrasound.

DOI: 10.21883/PSS.2023.02.55402.527

1. Introduction

Search for new spintronics materials [1,2] is a crucial task. Compounds having magnetoresistive effect in high temperature region offer wide application prospects [3–5]. In room temperature range, manganite semiconductors with colossal magnetoresistance in the vicinity of magnetic and charge ordering are well investigated [6–8].

Intensive experimental and theoretical research is focused on $R_{1-x}A_xMnO_3$ type transition metal oxides (R = La, Pr, Nd, Sm, etc., A = Ca, Sr, Ba, Pb) [9–14]. As bivalent ion concentration changes, manganite properties change significantly and a several phase transitions with various types of structural, magnetic, charge and orbital ordering are observed. In the phase transition region, kinetic performance changes and colossal magnetoresistance effect is observed [15,16]. The investigations are primarily focused on concentrations $x < 0.5$ due to the presence of colossal magnetoresistance effect in the high temperature range, therefore, they are favorable for spintronics applications.

Spatially-heterogeneous charge carrier density will result in exchange interaction modification and formation of complex magnetic structures and charge ordering. In the high concentration region, a perovskite-like structure in manganites exists for calcium ions only, and for A = Sr, Ba, Pb ions, hexagonal structure is implemented [9]. Doping of calcium ions in $CaMnO_3$ with rare earth elements results in the magnetic phase transition sequence and charge ordering at $x \sim 0.1$ above the Neel temperature [17].

Magnetoimpedance characteristics of $La_{0.67}Pb_{0.33}MnO_3$, prepared by sol-gel method differ from those of giant magnetoimpedance metallic materials. At low frequencies, the impedance demonstrates its peak in weal longitudinal field. The peak disappears in the high frequency region and drops dramatically as the magnetic field decreases. Magnetoimpedance in sol-gel nanocrystalline manganite depends both on the change in permittivity in the presence of magnetic field and on direct-current magnetoresistance [18]. Maximum magnetoimpedance occurs in the vicinity of the metal−insulator (MI) transition in $La_{2/3}Ba_{1/3}MnO_3$ and moves towards high temperatures in the external electric field [19]. The magnetoimpedance in $La_{0.67}Sr_{0.33-x}Pb_xMnO_3$ ($x = 0-0.33$) in the MI transition region is several times higher than the direct-current magnetoimpedance [20]. In manganites, the highest magnetoimpedance is achieved at MI phase transitions and when charge ordering. is formed.

In disordered $Me_xMn_{1-x}S$ (Me = Ag and Tm) semiconductors with non-isovalent substitution, magnetoimpedance and magnetoresistance were detected whose magnitude and sign depend on the electric field, temperature and type of substituting element [21]. In $Yb_xMn_{1-x}S$ ($0.05 < x < 0.2$), ytterbium ion is in trivalent state and maximum magnetoimpedance was detected in the vicinity of Jahn-Teller transition [22]. In $Lu_xMn_{1-x}S$ solid solution, negative direct-current magnetoresistance and critical temperature of electric polarization hysteresis disappearance [23]. Impedance reactance depends on the capacitance that is governed by permittivity. permittivity in electrically heterogeneous semoconductors shows magnetodielectric effect in the magnetic field [24–26].

The purpose of this research was to determine the influence of the heterogeneity caused by the increase in concentration of manganese ion substitution with lutetium ions in $Lu_xMn_{1-x}S$ on the impedance in magnetic field, on correlation of structure deformation and charge fluctuations with magnetoimpedance.

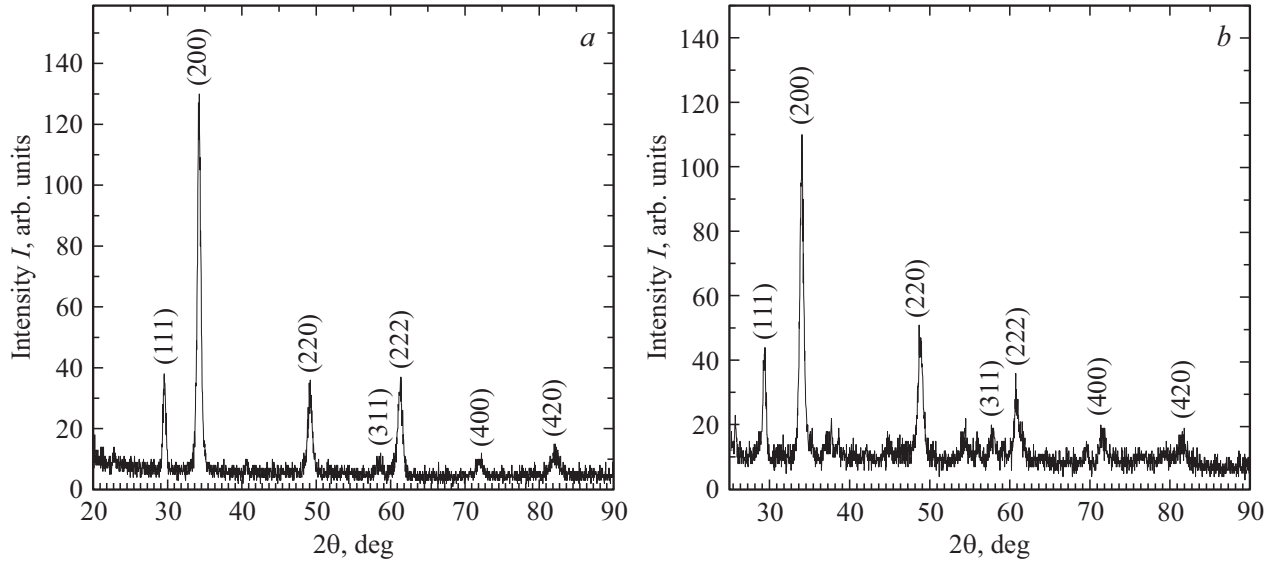

Figure 1. X-ray image of $Lu_xMn_{1-x}S$ for concentrations $x = 0.05$ (a), 0.1 (b).

2. Materials and methods

$Lu_xMn_{1-x}S$ solid solutions were grown by crystallization from moltenpowder sulphides in glassy carbon crucibles and quartz reactor in argon atmosphere by reactor pulling through a HF single-turn inductor. Sulphurization completeness was controlled by the X-ray diffraction analysis and weight checking methods. Phase composition and crystalline structure of synthesized specimens were investigated at room temperature using DRON-3 X-ray unit with CuK_α radiation in „point to point" data acquisition mode.

Figure 1 shows X-ray image of $Lu_xMn_{1-x}S$. The main peaks correspond to FCC-structure. For concentration $x \geq 0.1$, weak diffraction peaks induced by rhombic impurity phase occur.

Impedance resistance and reactance were measured using AM-3028 instrument in frequency range 0.1−1000 kHz and temperature range 80−500 K without any magnetic field and in magnetic field $H = 8$ kOe. Ultrasound attenuation was investigated on a $6 \times 5 \times 4$ mm specimen with two TsTS-19 piezoelectric transducers at a distance of $l = 4$ mm. A 100 ns rectangular pulse was applied to one of the piezoelectric transducers and voltage was recorded on the other transducer. Ultrasound attenuation factor was calculated as follows:

$$\alpha = \frac{\ln\left(\frac{U_{\text{in}}}{U_{\text{out}}}\right)}{l}, \qquad (1)$$

where U_{in} is the input voltage, U_{out} is the recorded voltage after sound transmission. Electrons (holes) interact with acoustic waves induced by piezoelectric transducers by means of deformation potential. Current carriers interact with ultrasound as a result of conductivity electron drag with progressive sound wave that will result in the difference of potentials across the specimen, acoustoelectric effect — electric sound.

3. Results and discussion

The magnitude of electrical state heterogeneity will be varied by the concentration of manganese substitution with lutetium. At low concentrations, trivalent lutetium ions are surrounded by manganese ions and form a random potential in the matrix. With concentration growth, lutetium ion clusters and regions with various charge carrier mobility are formed. Above the concentration of atom flow via FCC-lattice $X_c = 0.17$, domains with lutetium ions are formed and macroregions with different conductivity can be identified. Below the flow concentration, non-isovalent substitution results in formation of electrons and holes positioned in quantum wells. At the outer boundary of lutetium clusters, there are holes coupled by Coulomb interaction with electrons inside the cluster. Various types of charge carriers and degree of placement will result in different behavior of impedance components in the external magnetic field. Figure 2 shows impedance components at different frequencies vs. temperature.

In $Lu_{0.05}Mn_{0.95}S$, resistance $\mathrm{Re}(Z)$ and reactance $\mathrm{Im}(Z)$ demonstrate two extreme temperatures. Maximum temperature $\mathrm{Re}(Z)$ grows from $T = 344$ K for $\omega = 1$ kHz up to 356 K for $\omega = 300$ kHz. In the magnetic field, maximum temperature moves towards low temperatures. The second maximum $\mathrm{Re}(Z)$ and minimum $\mathrm{Im}(Z)$ temperature at 445 K does not depend on frequency. As a result of minimum impedance temperature displacement in the magnetic field, the magnetoimpedance changes sign from 4 to −60% (Figure 2, c, d). At frequencies above 50 kHz, impedance change is about 1%. Reactance is inversely proportional to

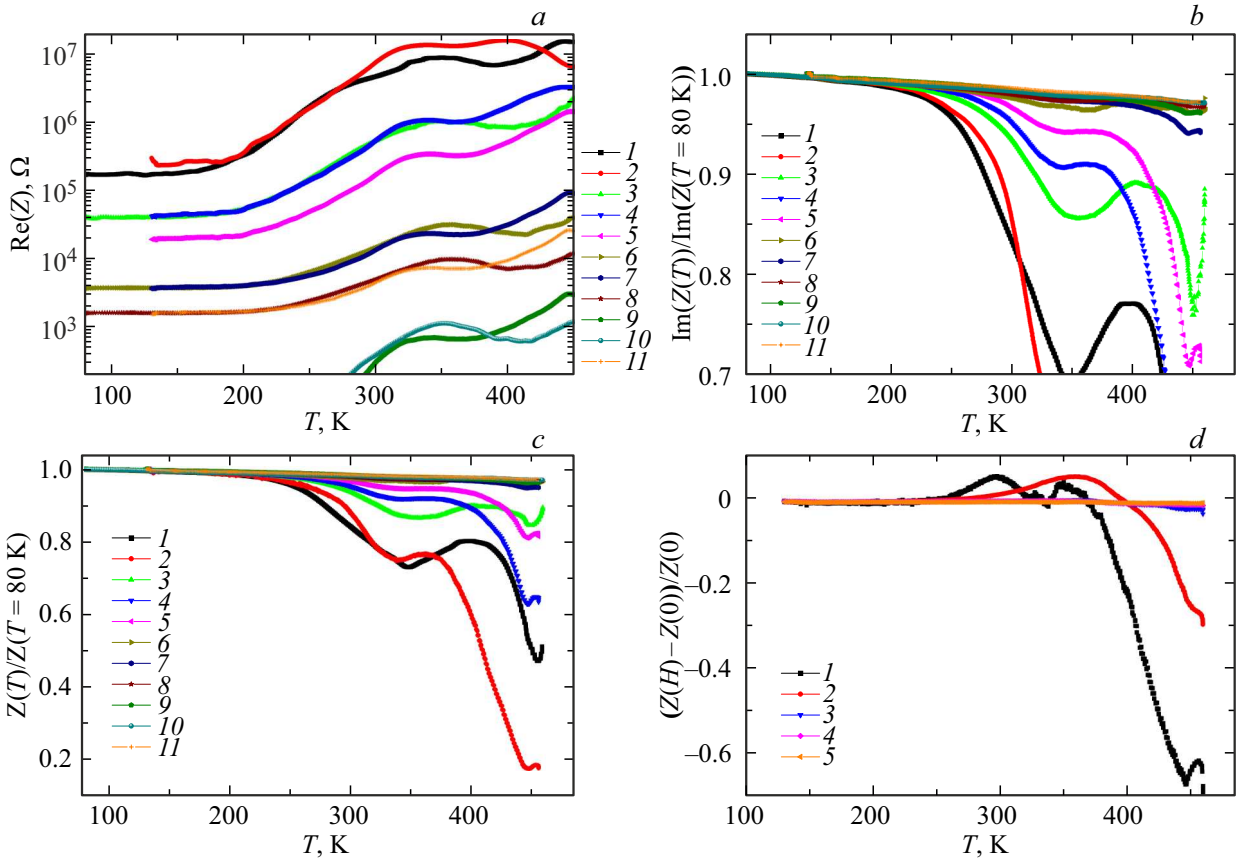

Figure 2. Resistance $\mathrm{Re}(Z)$ vs. temperature (a), specified reactance $\mathrm{Im}\big(Z(T)\big)/\mathrm{Im}\big(Z(T=80\,\mathrm{K})\big)$ (b) and specified impedance $Z(T)/Z(T=80\,\mathrm{K})$ (c) without field $(1, 3, 6, 8, 10)$ and in magnetic field $H = 8\,\mathrm{kOe}$ $(2, 4, 5, 7, 9, 11)$ at $\omega = 1\,\mathrm{kHz}$ $(1, 2)$, $5\,\mathrm{kHz}$ $(3, 4)$, $10\,\mathrm{kHz}$ (5), $50\,\mathrm{kHz}$ $(6, 7)$, $100\,\mathrm{kHz}$ $(8, 9)$, $300\,\mathrm{kHz}$ $(10, 11)$ for$\mathrm{Lu}_x\mathrm{Mn}_{1-x}\mathrm{S}$, $x = 0.05$. Temperature dependence of magnetoimpedance at $\omega = 1\,\mathrm{kHz}$ (1), $5\,\mathrm{kHz}$ (2), $50\,\mathrm{kHz}$ (3), $100\,\mathrm{kHz}$ (4), $300\,\mathrm{kHz}$ (5) for$\mathrm{Lu}_x\mathrm{Mn}_{1-x}\mathrm{S}$, $x = 0.05$.

capacitance $\mathrm{Im}(Z) \sim 1/C$, therefore the magnetoimpedance is caused by permittivity change in the magnetic field.

For concentration $x = 0.1$, direct-current resistance in $\mathrm{Lu}_x\mathrm{Mn}_{1-x}\mathrm{S}$ in the vicinity of the Neel temperature at $T = 120\,\mathrm{K}$ is more than by an order of magnitude higher, jump temperature is independent of frequency (Figure 3, *a*). Resistance increases dramatically above 410 K. In the magnetic field, the resistance gradually changes in the magnetic phase transition region and, with heating above 340–390 K, exceeds $\mathrm{Re}(Z)$ without field. The temperature at which $\mathrm{Re}\big(Z(H)\big) > \mathrm{Re}\big(Z(0)\big)$ increases with frequency growth.

Reactance as well as impedance decreases at $T = 119\,\mathrm{K}$ in a jump-like manner. The jump decreases sharply from 14% for $\omega = 1\,\mathrm{kHz}$, 2% for $\omega = 5\,\mathrm{kHz}$, and 0.3% for $\omega = 10\,\mathrm{kHz}$. In the magnetic field, the jump disappears. Reactance makes the major contribution to the magnetoimpedance. Dramatic changes in the impedance components in the vicinity of magnetic transition are caused by degenerated electron-hole states at LuS cluster boundary that are released by the magnetic field and spin orbital interaction. In magnetic-ordered state, holes on $\mathrm{Mn}^{2+\delta}$ and electrons on $\mathrm{Lu}^{3-\delta}$ form a certain type of orbital and charge ordering associated with sublattices in antiferromagnetic (AFM). Above the Neel temperature, orbital and charge order disappears at 430 K, where the impedance and reactance increase in a lump-like manner. The magnetoimpedance is shown in Figure 3, *d*.

Above the flow concentration, three macroregions with different conductivity and electron density may be identified: LuS and MnS domains and Mn–S–Lu interface. Figure 4 shows impedance components at different frequencies vs. temperature for $\mathrm{Lu}_x\mathrm{Mn}_{1-x}\mathrm{S}$, $x = 0.2$.

Direct-current resistance induced by electric loss reaches its peak during heating. The peak temperature grows with frequency. reactance decreases during heating and peak temperatures of derivative $d\mathrm{Im}(Z)/dT$ and resistance are the same. Temperature dependences of impedance components are described using the Cole–Cole model for permittivity [27]:

$$Z = \frac{A}{1 + (i\omega\tau)^{1-\alpha}}, \qquad (2)$$

where relaxation time τ is defined according to $\omega\tau = 1$. In the detail in Figure 4, dependence $\tau(1/T)$ is well

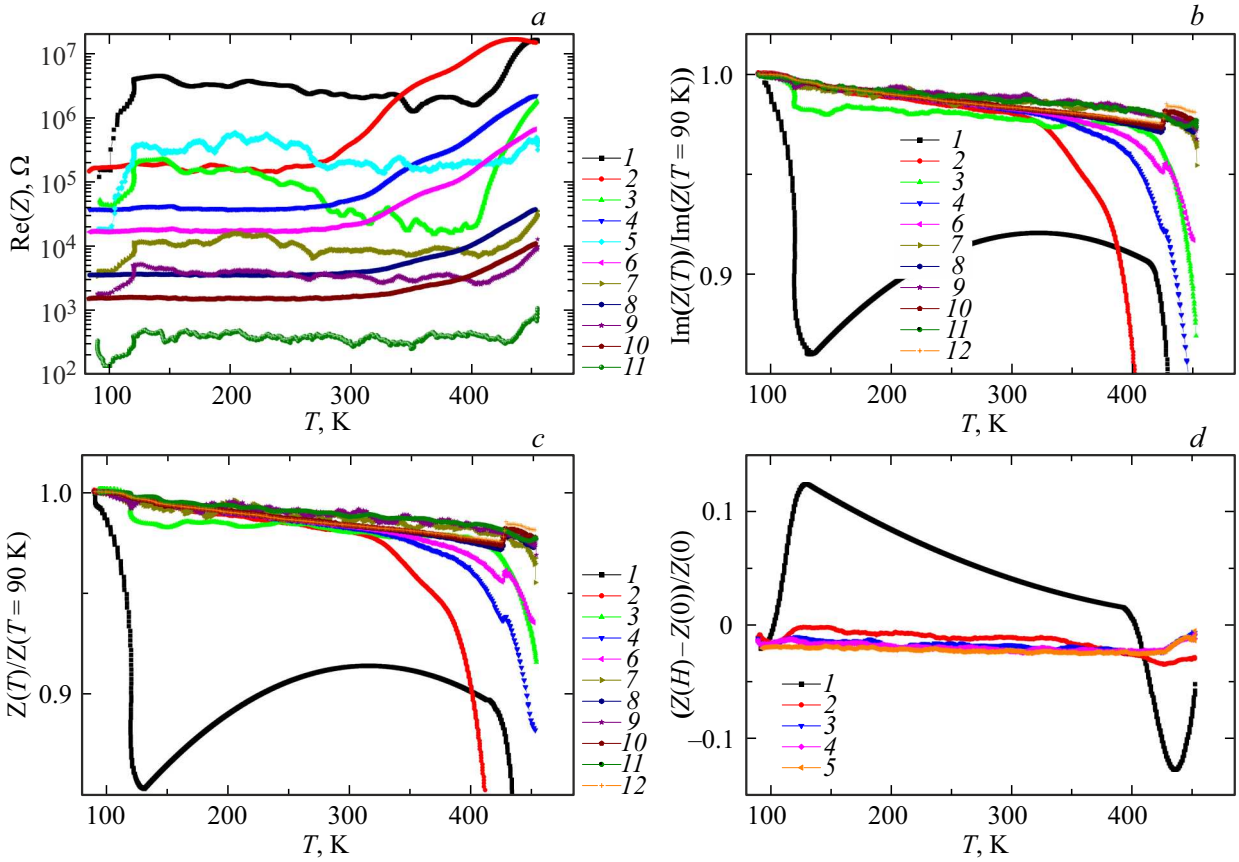

Figure 3. Resistance Re(Z) vs. temperature (a), specified reactance $\mathrm{Im}\big(Z(T)\big)/\mathrm{Im}\big(Z(T=90\,\mathrm{K})\big)$ (b) and specified impedance $Z(T)/Z(T=90\,\mathrm{K})$ (c) without field (*1, 3, 5, 7, 9, 11*) and in magnetic field $H = 8$ kOe (*2, 4, 6, 8, 10, 12*) at $\omega = 1$ kHz (*1, 2*), 5 kHz (*3, 4*), 10 kHz (*5, 6*), 50 kHz (*7, 8*), 100 kHz (*9, 10*), 300 kHz (*11, 12*) for $Lu_xMn_{1-x}S$, $x = 0.1$. Temperature dependence of magnetoimpedance at $\omega = 1$ kHz (*1*), 5 kHz (*2*), 50 kHz (*3*), 100 kHz (*4*), 300 kHz (*5*) for $Lu_xMn_{1-x}S$, $x = 0.1$.

described by exponential dependence $\tau = \tau_0 \cdot \exp(\Delta E/kT)$ with $\Delta E = 0.76$ eV without field and, in magnetic field $H = 8$ kOe, activation energy increases $\Delta E = 0.9$ eV. The exponential growth of relaxation time is caused by charge ordering. Probably at $T = 340$ K, charge ordering is formed at Mn–S–Lu cluster boundary and these clusters form the glass type state. The impedance significantly responds to the magnetic field above the charge ordering temperature in 10^3-10^5 Hz range. The major contribution to the magnetoimpedance is associated with reactance, in particular, with capacitance change in the magnetic field.

Transition caused by charge fluctuations will be expressed as dispersion of the imaginary part of impedance. Figure 5 shows frequency dependences Im(Z) for two limit temperatures. The reactance is governed by the capacitance and the Cole–Cole model for permittivity [28] is used to describe the frequency dependence:

$$\mathrm{Im}(Z) = Ar^{-1/2}\cos\theta, \tag{3}$$

$$r = \left[1 + (\omega\tau)^{1-\alpha}\sin\left(\frac{\alpha\pi}{2}\right)\right]^2 + \left[(\omega\tau_0)^{1-\alpha}\cos\left(\frac{\alpha\pi}{2}\right)\right]^2, \tag{4}$$

$$\theta = \mathrm{arctg}\left[\frac{(\omega\tau_0)^{1-\alpha}\cos\left(\frac{\alpha\pi}{2}\right)}{1 + (\omega\tau_0)^{1-\alpha}\sin\left(\frac{\alpha\pi}{2}\right)}\right]. \tag{5}$$

Exponent α describes increase in dispersion and $\alpha = 0$ corresponds to the Debye model. At room temperature, adjustment $\mathrm{Im}\big(Z(\omega)\big)$ by function (3) gives exponent $\alpha = 0.025$ (Figure 5, b). When heated to 340 K, dispersion $\mathrm{Im}\big(Z(\omega)\big)$ in $Lu_{0.2}Mn_{0.8}S$ increases up to $\alpha = 0.05$ and remains almost unchanged up to 420 K and increased up to $\alpha = 0.1$ above this temperature. In the Debye model, one relaxation time is used, in the disordered system, there is a relaxation time spectrum which can be qualitatively described by a single parameter α that shows expansion of relaxation time distribution. For concentration below the flow concentration, frequency dependences $\mathrm{Im}\big(Z(\omega)\big)$ are not described within the Cole–Cole model, except $T = 460$ K (Figure 5, a).

Structural, magnetic and charge transitions will be manifested in ultrasound attenuation. Figure 6 shows ultrasound attenuation factor in temperature range 80–500 K. Low-temperature peaks $\alpha(T)$ at $T = 138$ K, $x = 0.05$ and $T = 113$ K, $x = 0.2$ are observed in the magnetic phase

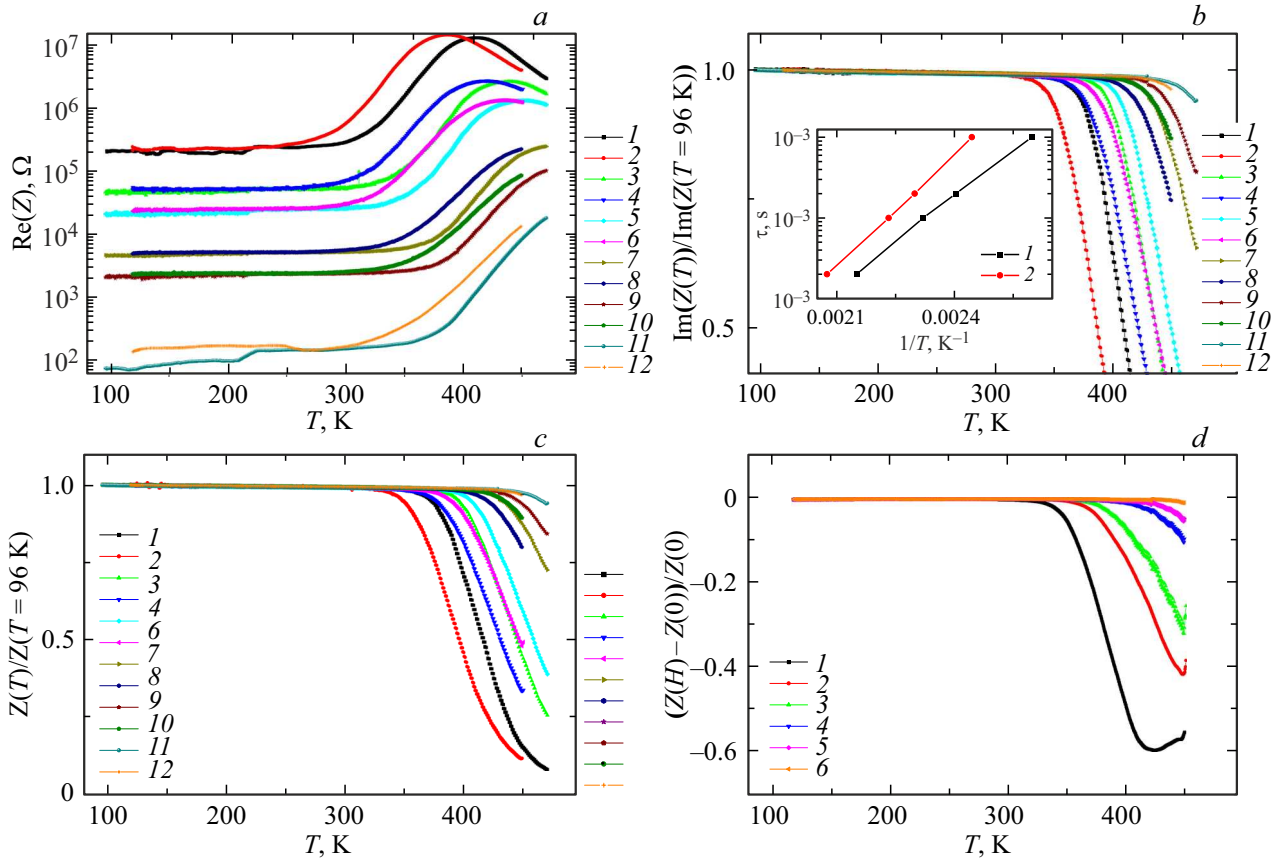

Figure 4. Resistance $\mathrm{Re}(Z)$ vs. temperature (*a*), specified reactance $\mathrm{Im}\big(Z(T)\big)/\mathrm{Im}\big(Z(T=96\,\mathrm{K})\big)$ (*b*) and specified impedance $Z(T)/Z(T=96\,\mathrm{K})$ (*c*) without field (*1, 3, 5, 7, 9, 11*) and in magnetic field $H = 8$ kOe (*2, 4, 6, 8, 10, 12*) at $\omega = 1$ kHz (*1, 2*), 5 kHz (*3, 4*), 10 kHz (*5, 6*), 50 kHz (*7, 8*), 100 kHz (*9, 10*), 300 kHz (*11, 12*) for $Lu_xMn_{1-x}S$, $x = 0.2$. Temperature dependence of magnetoimpedance at $\omega = 1$ kHz (*1*), 5 kHz (*2*), 10 kHz (*3*), 50 kHz (*4*), 100 kHz (*5*), 300 kHz (*6*) for $Lu_xMn_{1-x}S$, $x = 0.2$. Detail: relaxation time vs. reciprocal temperature.

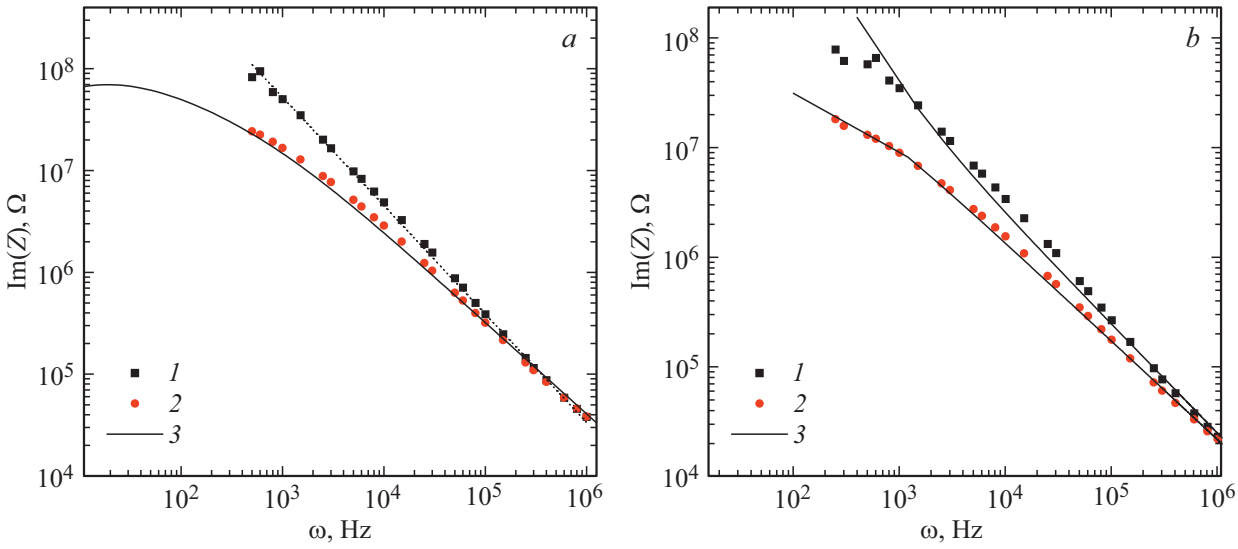

Figure 5. Reactance $\mathrm{Im}(Z)$ vs. frequency ω for $Lu_xMn_{1-x}S$ with $x = 0.1$ (*a*), 0.2 (*b*) at $T = 300$ K (*1*), 460 K (*2*). Adjustment functions (*3*) according to equations (3–5).

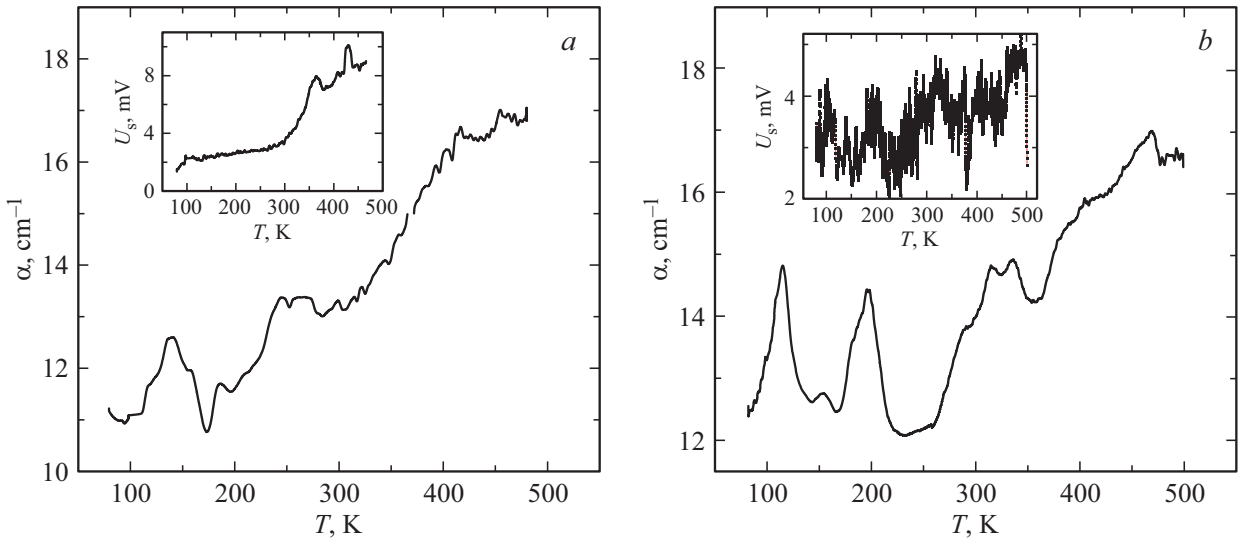

Figure 6. Temperature dependence of ultrasound attenuation factor α for $Lu_xMn_{1-x}S$ with $x = 0.05$ (a), 0.2 (b). Detail: electric sound U_s vs. temperature in $Lu_xMn_{1-x}S$ with $x = 0.1$ (a), 0.2 (b).

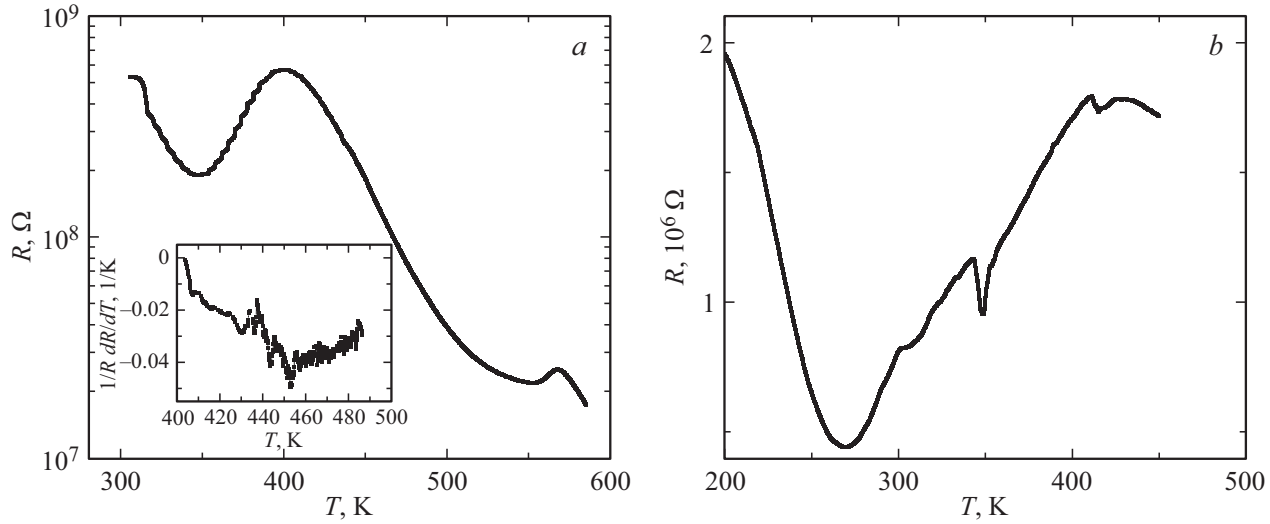

Figure 7. Temperature dependence of resistance for $Lu_xMn_{1-x}S$ with $x = 0.05$ (a), 0.2 (b). Detail: Temperature dependence $1/R\ dR/dT$ for $Lu_xMn_{1-x}S$ with $x = 0.05$.

transition region and are associated with the lattice strain caused by magnetoelastic interaction. Peak of $\alpha(T)$ and electric sound at $T = 200\,\mathrm{K}$ in $Lu_{0.2}MnO_{0.8}S$ was probably caused by structural transition. Acoustic phonons excited by piezoelectric transducer drag the electrons and produce difference of potentials across the specimen. Formation of hole charge ordering at LuS−MnS intercluster interface causes peaks in $\alpha(T)$ and eletric sound at $T = 330\,\mathrm{K}$. At this temperature, the reactance dispersion grows and direct-current resistance reaches the peak at 340 K (Figure 7, b).

A minor jump in $\alpha(T)$ at $T = 452\,\mathrm{K}$ at $x = 0.05$ coincides with minimum temperature $\mathrm{Im}\big(Z(T)\big)$ and maximum capacitance. resistance temperature coefficient $1/R\ dR/dT$ also reaches its minimum at the same temperature (Detail in Figure 7, a). The use of various methods: ultrasound attenuation, impedance and direct-current resistance give abnormal condition at the same temperature. At this temperature, local structure distortions probably occur in the vicinity of lutetium ions and result in electron structure change. The electric sound reaches sharp peak at 440 K. Above the flow concentration at $x = 0.2$, sound and electric sound attenuation peak moves into the high temperature region up to $T = 470\,\mathrm{K}$. Ultrasound attenuation peaks at 400−420 K and the absence of abnormal electric sound at these temperatures are caused by charged defect ordering at which current carriers undergo dispersion and maximum resistance (Figure 7).

4. Conclusion

In manganese sulfides substituted with lutetium, the major contribution to the impedance is governed by the reactance. The maximum ultrasound attenuation was detected in the magnetic phase transition region as a result of magnetoelastic interaction. Two charge ordering temperatures were determined from the electric sound. At low concentrations, charge ordering is accompanied by the capacitance peak and increase in the reactance in the magnetic field. Minimum reactance and maximum resistance displacement vs. temperature in the magnetic field results in the change of magnetoimpedance sign in the vicinity of the transition. At high lutetium concentrations, impedance dispersion grows with impedance components described in the Cole−Cole model. At high temperatures, the attenuation peak is associated with the charged vacancy ordering temperature accompanied with the resistance peak vs. temperature and impedance decrease in the magnetic field.

Funding

This study was supported by a grant of the President of the Russian Federation No. MK-620.2021.1.2.

Conflict of interest

The authors declare that they have no conflict of interest.

References

[1] I. Zutic, J. Fabian, S. Das Sarma. Rev. Mod. Phys. **76**, 323 (2004). https://doi.org/10.1103/RevModPhys.76.323
[2] A. Fert. UFN, **178**, 1336 (2008). (in Russian).
[3] S.S. Aplesnin, M.N. Sitnikov. JETP Lett. **100**, 95 (2014). https://doi.org/10.1134/S0021364014140021
[4] O.B. Romanova, V.V. Kretinin, S.S. Aplesnin, M.N. Sitnikov, L.V.. Udod, K.I. Yanushkevich. FTT, **63**, 721 (2021). (in Russian).
[5] M. Kreutzbruck, B. Mogwitz, F. Gruhl, L. Kienle, C. Korte, J. Janek. Appl. Phys. Lett. **86**, 072102 (2005). https://doi.org/10.1063/1.1866642
[6] E.L. Nagaev. UFN, **166**, 833 (1996). (in Russian).
[7] M.Yu. Kagan, K.L. Kugel. UFN, **171**, 577 (2001). (in Russian).
[8] Yu.A. Izyumov, Yu.N. Skryabin. UFN, **171**, 121 (2001). (in Russian).
[9] R. Gunnarsson, M. Hanson. Phys. Rev. B **73**, 014435 (2006). https://doi.org/10.1103/PhysRevB.73.014435
[10] Yu.A. Boikov, T. Kleason, V.A. Danilov. FTT, **47**, 2189 (2005). (in Russian).
[11] S.L. Cheng, C.H. Du, T.H. Chuang, J.G. Lin. Sci. Rep. **9**, 7828 (2019). https://doi.org/10.1038/s41598-019-44104-7
[12] A. Asamitsu, Y. Tomioka, H. Kuwahara, Y. Tokura. Nature **388**, 50 (1997). https://doi.org/10.1038/40363
[13] N.G. Bebenin, R.I. Zainullina, V.V. Ustinov. UFN, **188**, 801 (2018). (in Russian).
[14] M. Hsini, L. Ghivelder, F. Parisi. JMMM **535**, 168059 (2021). https://doi.org/10.1016/j.jmmm.2021.168059
[15] J. Tao, D. Niebieskikwiat, M. Varela, W. Luo, M.A. Schofield, Y. Zhu, M.B. Salamon, J.M. Zuo, S.T. Pantelides, S.J. Pennycook. Phys. Rev. Lett. **103**, 097202 (2009). https://doi.org/10.1103/PhysRevLett.103.097202
[16] J. Wu, J.W. Lynn, C.J. Glinka, J. Burley, H. Zheng, J.F. Mitchell, C. Leighton. Phys. Rev. Lett. **94**, 037201 (2005). https://doi.org/10.1103/PhysRevLett.94.037201
[17] W.E. Pickett, D.J. Singh. Phys. Rev. B **53**, 1146 (1996). https://doi.org/10.1103/PhysRevB.53.1146
[18] H. Qin, J. Hu, B. Li, Y. Hao, J. Chen, M. Jiang. JMMM **320**, 2770 (2008). https://doi.org/10.1016/j.jmmm.2008.06.011
[19] J. Hu, H. Qin, H. Niu, L. Zhu, J. Chen, W. Xiao, Yu. Pei. JMMM **261**, 105 (2003). https://doi.org/10.1016/S0304-8853(02)01430-0
[20] S. Biswas, S. Keshri. Phase Transitions **92**, 172 (2019). https://doi.org/10.1080/01411594.2019.1566826
[21] O.B. Romanova, S.S. Aplesnin, M.N. Sitnikov, L.V. Udod. JETP **132**, 831 (2021). http://doi.org/10.1134/S106377612103016X
[22] S.S. Aplesnin, M.N. Sitnikov, A.M. Kharkov, S.O. Konovalov, A.M. Vorotinov. JMMM **513**, 167104 (2020). https://doi.org/10.1016/j.jmmm.2020.167104
[23] S.S. Aplesnin, M.N. Sitnikov, A.M. Kharkov, O.B. Begisheva, F.V. Zelenov. Phys. Status Solidi B **259**, 2100555 (2022). https://doi.org/10.1002/pssb.202100555
[24] M.M. Parish, P.B. Littlewood. Phys. Rev. Lett. **101**, 166602 (2008). https://doi.org/10.1103/PhysRevLett.101.166602
[25] M.M. Parish. Phil. Trans. R. Soc. A **372**, 20120452 (2014). http://doi.org/10.1098/rsta.2012.0452
[26] S.S. Aplesnin, A.N. Masyugin, V.V. Kretinin, S.O. Konovalov, N.P. Shestakov. Phys. Solid State **63**, 242 (2021). https://doi.org/10.1134/S1063783421020025
[27] K.S. Cole, R.H. Cole. J. Chem. Phys. **9**, 341 (2004). https://doi.org/10.1063/1.1750906
[28] A.S. Volkov, G.D. Koposov, R.O. Perfilyev. FTT, **125**, 364 (2018). (in Russian).